

Supplementary Information

A Cyanide-Bridged Di-Manganese Carbonyl Complex that Photochemically Reduces CO₂ to CO

Hsin-Ya Kuo, Tia S. Lee, An T. Chu, Steven E. Tignor.

Gregory D. Scholes, and Andrew B. Bocarsly*

Department of Chemistry, Princeton University, Princeton, New Jersey 08544, United States

*Email: bocarsly@princeton.edu

Contents

ATR-IR infrared spectra of complexes 1 , 2 and 3	S2
Temperature dependent ¹ H-NMR of 1	S2
Cyclic voltammetry of complex 1 at various switching potential window.....	S2
Nicholson and Shain diagnostics of 1	S3
Proton content and product analysis of 1	S3
Post bulk electrolysis ¹ H-NMR of 1	S4
CV Simulations by DigiElch of 1	S5
³¹ P-NMR of 1 and IR spectral changes post photolysis.....	S6
UV-vis spectral comparison of 1 under CO ₂ condition under photolysis.....	S6
¹ H-NMR and of 1	S7
¹³ C-NMR and of 1	S7
X-Ray Crystallography Data of 1	S8-12

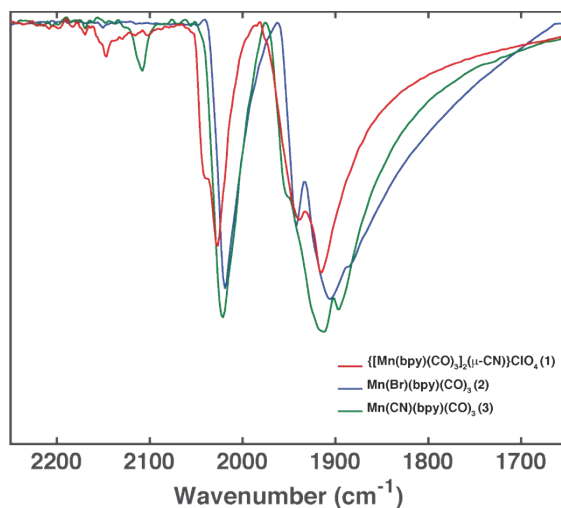


Figure S1 ATR-IR infrared spectra of complexes **1** (red), **2** (blue) and **3** (green).

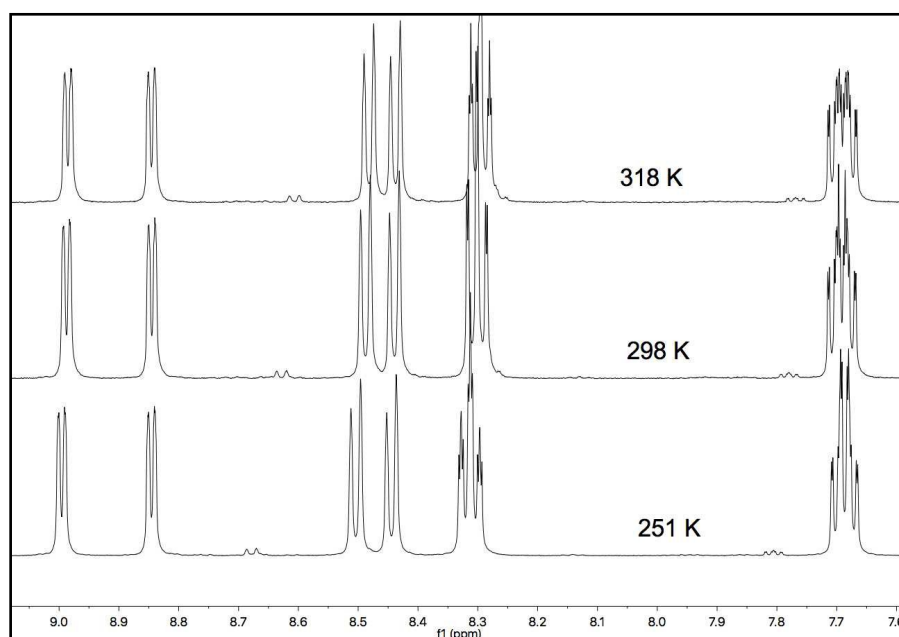


Figure S2 The 1H -NMR spectra of aromatic protons of complex **1** in d-acetone at selected temperatures.

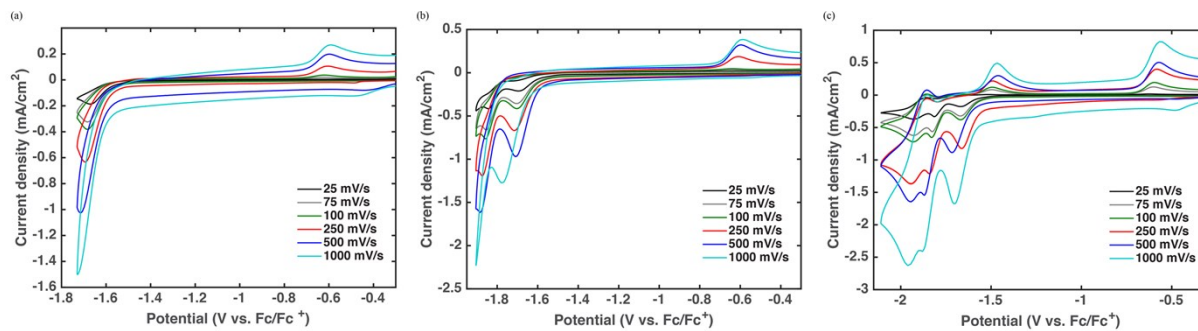


Figure S3 Cyclic voltammetry of complex **1** (1mM) under Ar in dry MeCN with 0.1M TBAP supporting electrolyte. The switching potential was set to (a) -1.74 V vs. Fc/Fc^+ , (b) -1.88 V vs. Fc/Fc^+ , (c) -2.12 V vs. Fc/Fc^+ .

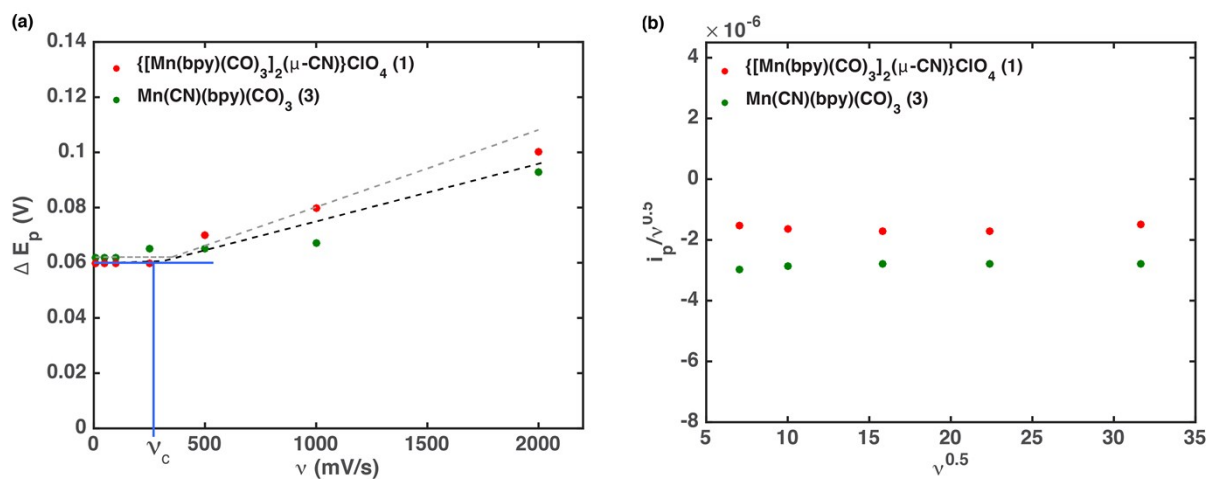


Figure S4 (a) Plot of the peak-to-peak separation, ΔE_p , as a function of scan rate shows the transition from reversible to quasi-reversible charge transfer kinetics at ν_c . (b) Plot of the current function, given by $i_p/\nu^{0.5}$, as a function of square root of scan rate shows the reversible electron transfer process for complex **1** and **3** at $V = -1.92$ V and -1.93 V vs. Fc/Fc^+ , respectively.

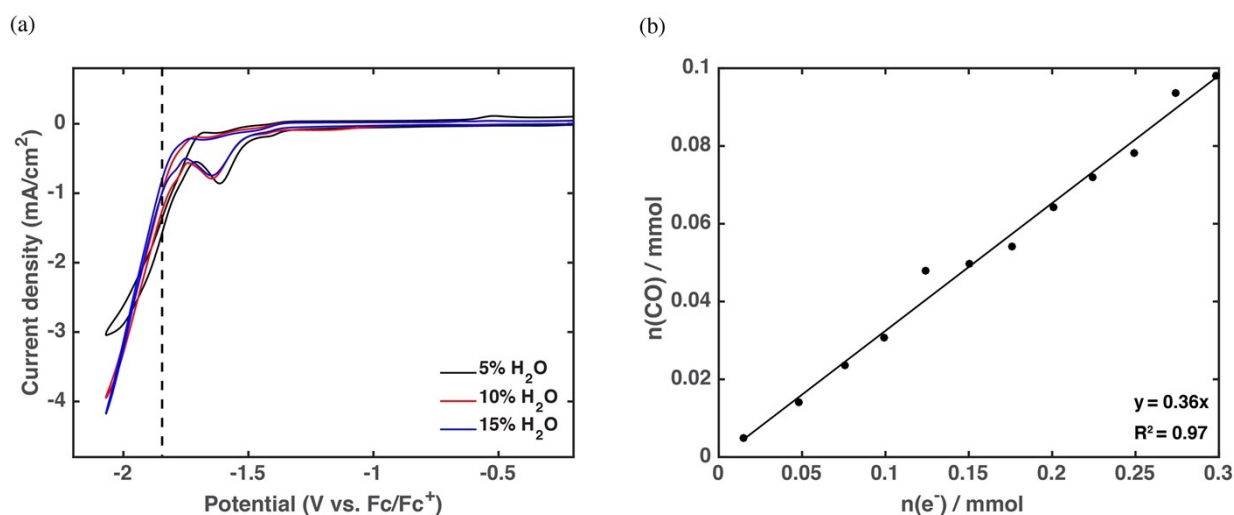


Figure S5 (a) CV of **1** with increased amount of H_2O added under CO_2 atmosphere at 250 mV/s and the dashed line indicates the position of the second peak potential at -1.85 V vs Fc/Fc^+ in the dry electrolyte. (b) CO production versus the number of electrons consumed. The slope represents a Faradaic efficiency of $72\% \pm 2.6\%$. Data were collected at -1.85 V vs Fc/Fc^+ with solutions of the complex **1** (1 mM) loaded in CO_2 -saturated 0.1 M TBAP in MeCN with 5% H_2O .

CV Simulations

Simulations of the experimental CV data were performed using DigiElch 4.0 based on the proposed mechanism. The reaction parameters listed in the table S1 were obtained using the program's non-linear regression fitting procedure on the CV data at 250 mV/s. For other scanning rates, we take the optimized parameters from 250 mV/s as the initial guess for further refinement. The value of the working electrode area (0.0707 cm²) and the scan rate were imported directly into each experimental CV, and all simulations performed excluded data points positive of -0.9 V vs Fc/Fc⁺. The double layer capacitance for each experimental scan was estimated to be 10 μF, except for the 750 mV/s scan which was estimated to be 15 μF.

Table S1. Kinetic constants and diffusion constants for the reduction steps of interest

Reaction Step	α	k_s (cm/s)	D (10 ⁻⁵ cm ² /s)
$\begin{array}{c} [\text{Mn-C}\equiv\text{N-Mn}]^+ \\ \mathbf{1} \end{array} \xrightarrow[-1.68 \text{ V}]{+e^-} \begin{array}{c} [\text{Mn-C}\equiv\text{N-Mn}]^\cdot \\ \mathbf{Mn}^- \end{array}$	0.67	0.19	$\mathbf{1}$: 2.34 \mathbf{Mn}^- : 2.28
$\begin{array}{c} [\text{Mn-C}\equiv\text{N-Mn}]^\cdot \\ \mathbf{Mn}^- \end{array} \xrightarrow[+\text{MeCN}]{-\text{CO}} \begin{array}{c} \text{solvato complex} \\ \mathbf{MnA}^- \end{array}$	-	-	\mathbf{MnA}^- : 1.00
$\mathbf{MnA}^- \xrightarrow[-1.85 \text{ V}]{+e^-} \mathbf{MnA}^{2-}$	0.61	1.11	\mathbf{MnA}^{2-} : 0.75

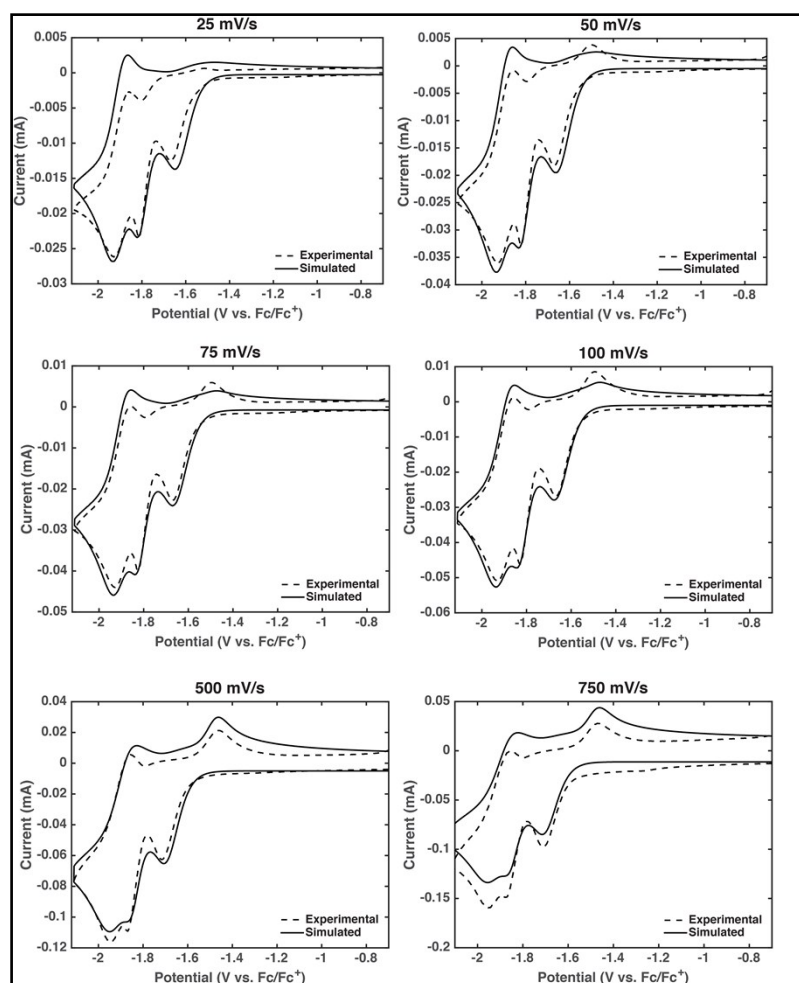


Figure S7 A complete DigiElch modeling of cyclic voltammetry at various scan rate

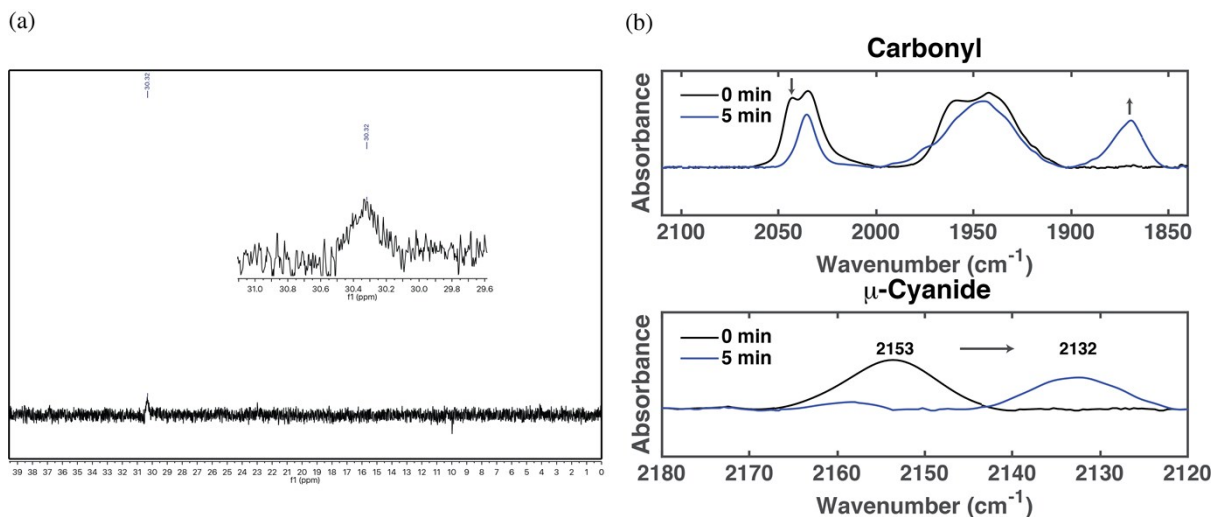


Figure S8 (a) The ^{31}P -NMR spectrum in d-MeCN for complex **1** (2mM), and PPh_3 (0.2 mM) after 5 min irradiation with 365 nm 3W LED. The CO-loss reaction is also supported by using low concentrations of the substituting ligand, i.e, PPh_3 . The ^{31}P NMR spectrum shows one signal at 30.3 ppm belonging to coordinated PPh_3 . (b) The IR spectral comparison of pre- and 4 min irradiation of **1** and PPh_3 in MeCN. All other experiment conditions remained fixed. Changes of carbonyl and bridged-cyanide stretching bands are indicated with arrows. Disappearance of one of the two higher CO stretching modes further supports the loss of CO in the reaction. The CN band shifts to lower energy upon photolysis, which is consistent with bridged-CN stretch, suggests the integrity of the CN-bridged structure.

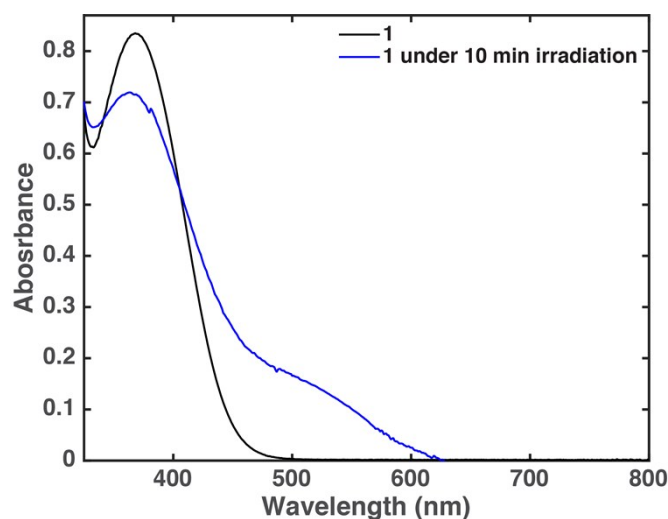
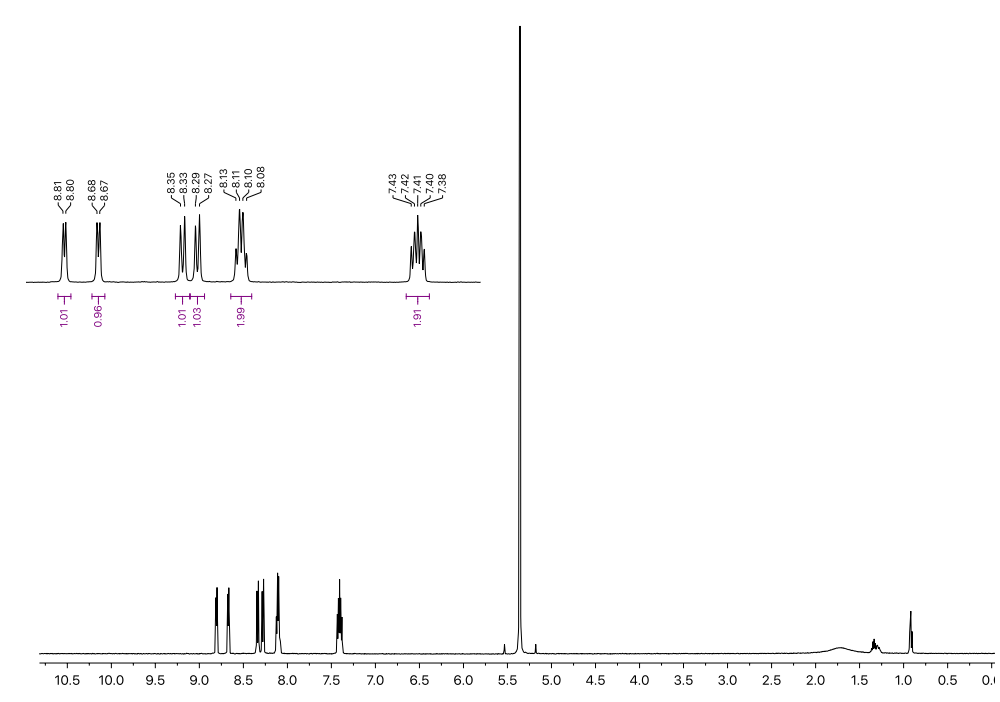


Figure S9 UV-vis spectral comparison of **1** in MeCN (black trace) and **1** in CO_2 -saturated 1M PhOH/MeCN upon 10 min photolysis with 395 nm LED light (blue trace). No dimer formation is observed between 600 and 800 nm, and a shoulder peak around 500 nm is consistent with the previous photolysis study shown in Figure 7c.

^1H NMR of **1**

Temperature: 22 °C

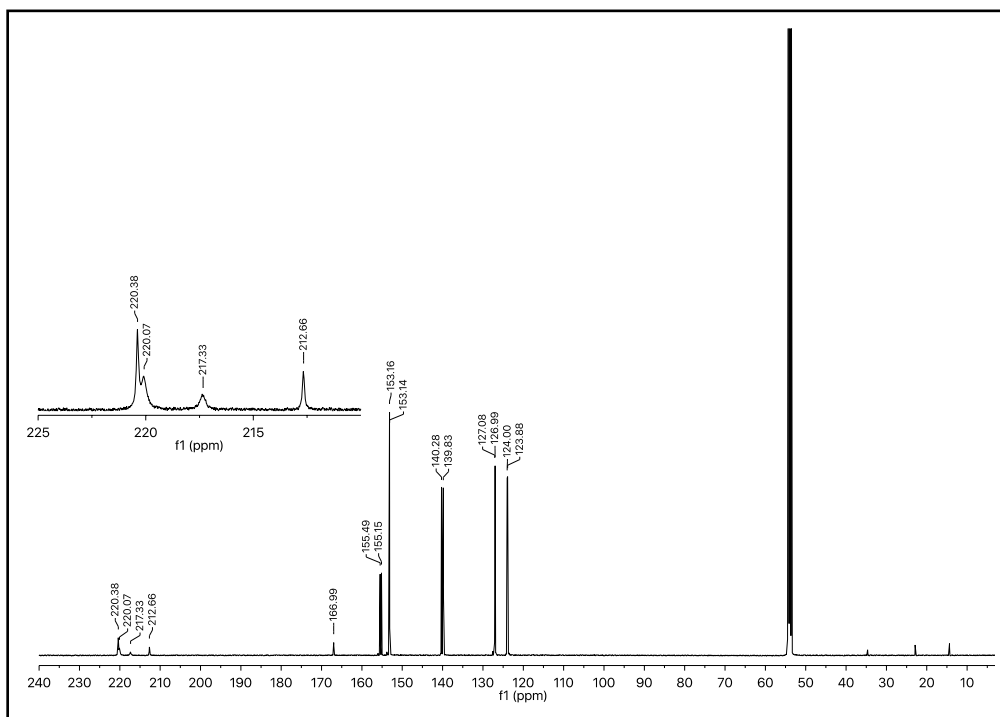
Solvent: Dichloromethane- d_2



^{13}C NMR of **1**

Temperature: 22 °C

Solvent: Dichloromethane- d_2



X-ray Crystallography

A single crystal suitable for X-ray diffraction analysis of the complex **1** was isolated by slow diffusion of hexane into a dichloromethane solution at room temperature which results in the formation of pale yellow specimen. Single X-ray diffraction intensity data were collected on with a Bruker Photon 100 CMOS detector using Mo K α radiation. The frames were integrated with the Bruker SAINT software package using a narrow-frame algorithm.

Collection Data for **1**

Formula: C₂₉H₂₀Cl₅Mn₂N₅O₁₀

Formula Weight: 885.63 g/mol

Crystal System: monoclinic

Space Group: P 1 21/n 1

Unit Cell Dimensions:

$$\begin{aligned} a &= 11.0681(4) \text{ \AA} & \alpha &= 90 \text{ degrees} \\ b &= 30.9567(10) \text{ \AA} & \alpha &= 115.7260(10) \text{ degrees} \\ c &= 11.5924(4) \text{ \AA} & \gamma &= 90 \text{ degrees} \end{aligned}$$

Cell Volume: 3578.2(2) \AA^3

Temperature: 100 K

Radiation Type: MoK α

Radiation Wavelength: 0.71073 \AA

Theta range for data collection: 2.06 degrees to 33.14 degrees

Reflections Collected: 97453

Goodness-of-fit on F²: 1.123

Bond Lengths (\AA):

Mn1	N1	2.047(1)
Mn1	N2	2.053(1)
Mn1	C11	1.810(2)
Mn1	C12	1.809(1)
Mn1	C13	1.840(2)
Mn1	C27A	2.06(2)
O1	C11	1.149(2)
N1	C1	1.343(2)
N1	C5	1.349(2)
C1	H1	0.949
C1	C2	1.383(2)
Mn2	N3	2.044(1)
Mn2	N4	2.045(1)
Mn2	C24	1.808(2)
Mn2	C25	1.812(2)
Mn2	C26	1.817(2)
Mn2	N5A	1.96(1)
O2	C12	1.149(2)
N2	C6	1.354(2)
N2	C10	1.343(2)
C2	H2	0.95

C2	C3	1.381(3)
O3	C13	1.141(2)
N3	C14	1.344(2)
N3	C18	1.352(2)
C3	H3	0.95
C3	C4	1.381(3)
O4	C24	1.146(2)
N4	C19	1.349(2)
N4	C23	1.345(2)
C4	H4	0.949
C4	C5	1.389(2)
O5	C25	1.144(2)
C5	C6	1.474(2)
O6	C26	1.146(2)
C6	C7	1.392(3)
C7	H7	0.951
C7	C8	1.384(3)
C8	H8	0.95
C8	C9	1.383(2)
C9	H9	0.95
C9	C10	1.387(3)
C10	H10	0.949
C14	H14	0.95
C14	C15	1.387(2)
C15	H15	0.95
C15	C16	1.383(2)
C16	H16	0.951
C16	C17	1.388(2)
C17	H17	0.95
C17	C18	1.385(2)
C18	C19	1.476(2)
C19	C20	1.391(2)
C20	H20	0.95
C20	C21	1.388(3)
C21	H21	0.95
C21	C22	1.381(3)
C22	H22	0.95
C22	C23	1.387(3)
C23	H23	0.951
C27A	N5A	1.13(2)
C12	C28	1.771(2)
C13	C28	1.767(2)
C28	H28A	0.99

C28 H28B 0.989

Bond Angles (degrees):

N1	Mn1	N2	78.68(5)
N1	Mn1	C11	96.16(6)
N1	Mn1	C12	175.38(7)
N1	Mn1	C13	92.17(7)
N1	Mn1	C27A	85.8(5)
N2	Mn1	C11	173.25(7)
N2	Mn1	C12	96.74(6)
N2	Mn1	C13	92.82(6)
N2	Mn1	C27A	86.1(5)
C11	Mn1	C12	88.36(7)
C11	Mn1	C13	91.72(7)
C11	Mn1	C27A	89.2(5)
C12	Mn1	C13	88.60(7)
C12	Mn1	C27A	93.4(5)
C13	Mn1	C27A	177.8(5)
Mn1	N1	C1	125.5(1)
Mn1	N1	C5	116.3(1)
C1	N1	C5	118.2(1)
N1	C1	H1	118.5
N1	C1	C2	123.0(2)
H1	C1	C2	118.5
N3	Mn2	N4	79.03(5)
N3	Mn2	C24	95.63(6)
N3	Mn2	C25	177.04(6)
N3	Mn2	C26	95.00(6)
N3	Mn2	N5A	86.0(4)
N4	Mn2	C24	174.57(7)
N4	Mn2	C25	98.15(6)
N4	Mn2	C26	92.63(6)
N4	Mn2	N5A	85.4(4)
C24	Mn2	C25	87.18(7)
C24	Mn2	C26	88.76(7)
C24	Mn2	N5A	93.4(4)
C25	Mn2	C26	86.01(7)
C25	Mn2	N5A	92.8(4)
C26	Mn2	N5A	177.5(4)
Mn1	N2	C6	115.8(1)
Mn1	N2	C10	125.9(1)
C6	N2	C10	118.2(1)
C1	C2	H2	120.6
C1	C2	C3	118.6(2)

H2	C2	C3	120.8
Mn2	N3	C14	126.0(1)
Mn2	N3	C18	115.9(1)
C14	N3	C18	118.1(1)
C2	C3	H3	120.5
C2	C3	C4	119.1(2)
H3	C3	C4	120.4
Mn2	N4	C19	115.7(1)
Mn2	N4	C23	125.5(1)
C19	N4	C23	118.7(1)
C3	C4	H4	120.3
C3	C4	C5	119.4(2)
H4	C4	C5	120.3
N1	C5	C4	121.7(2)
N1	C5	C6	114.5(1)
C4	C5	C6	123.8(2)
N2	C6	C5	114.8(1)
N2	C6	C7	121.9(2)
C5	C6	C7	123.3(2)
C6	C7	H7	120.4
C6	C7	C8	119.3(2)
H7	C7	C8	120.3
C7	C8	H8	120.5
C7	C8	C9	118.9(2)
H8	C8	C9	120.6
C8	C9	H9	120.4
C8	C9	C10	119.0(2)
H9	C9	C10	120.6
N2	C10	C9	122.7(2)
N2	C10	H10	118.7
C9	C10	H10	118.6
Mn1	C11	O1	177.5(1)
Mn1	C12	O2	177.7(1)
Mn1	C13	O3	177.0(2)
N3	C14	H14	118.6
N3	C14	C15	122.9(1)
H14	C14	C15	118.5
C14	C15	H15	120.7
C14	C15	C16	118.7(2)
H15	C15	C16	120.7
C15	C16	H16	120.5
C15	C16	C17	119.0(2)
H16	C16	C17	120.5

C16	C17	H17	120.3
C16	C17	C18	119.3(2)
H17	C17	C18	120.4
N3	C18	C17	122.0(1)
N3	C18	C19	114.3(1)
C17	C18	C19	123.7(1)
N4	C19	C18	115.0(1)
N4	C19	C20	122.0(2)
C18	C19	C20	123.0(2)
C19	C20	H20	120.6
C19	C20	C21	118.8(2)
H20	C20	C21	120.6
C20	C21	H21	120.4
C20	C21	C22	119.3(2)
H21	C21	C22	120.4
C21	C22	H22	120.5
C21	C22	C23	118.9(2)
H22	C22	C23	120.6
N4	C23	C22	122.3(2)
N4	C23	H23	118.8
C22	C23	H23	118.9
Mn2	C24	O4	176.6(2)
Mn2	C25	O5	175.0(1)
Mn2	C26	O6	173.4(1)
Mn1	C27A	N5A	174(2)
Mn2	N5A	C27A	171(1)
Cl2	C28	Cl3	110.9(1)
Cl2	C28	H28A	109.3
Cl2	C28	H28B	109.4
Cl3	C28	H28A	109.5
Cl3	C28	H28B	109.5
H28A	C28	H28B	108.1